Analysis of proteome adaptation reveals a key role of the bacterial envelope in starvation survival

Severin Schink[1, *, #], Constantin Ammar[1,2,*], Yu-Fang Chang[1],
Ralf Zimmer[2] and Markus Basan[1, #]

[1] Systems Biology Department, Harvard Medical School, 200 Longwood Ave, 02115 MA, USA
[2] Institute of Informatics, Ludwig-Maximilians-Universität München, Amalienstr. 17, 80333, Munich, Germany
* Contributed equally
[#] Correspondence: info@severin-schink.eu and markus@hms.harvard.edu

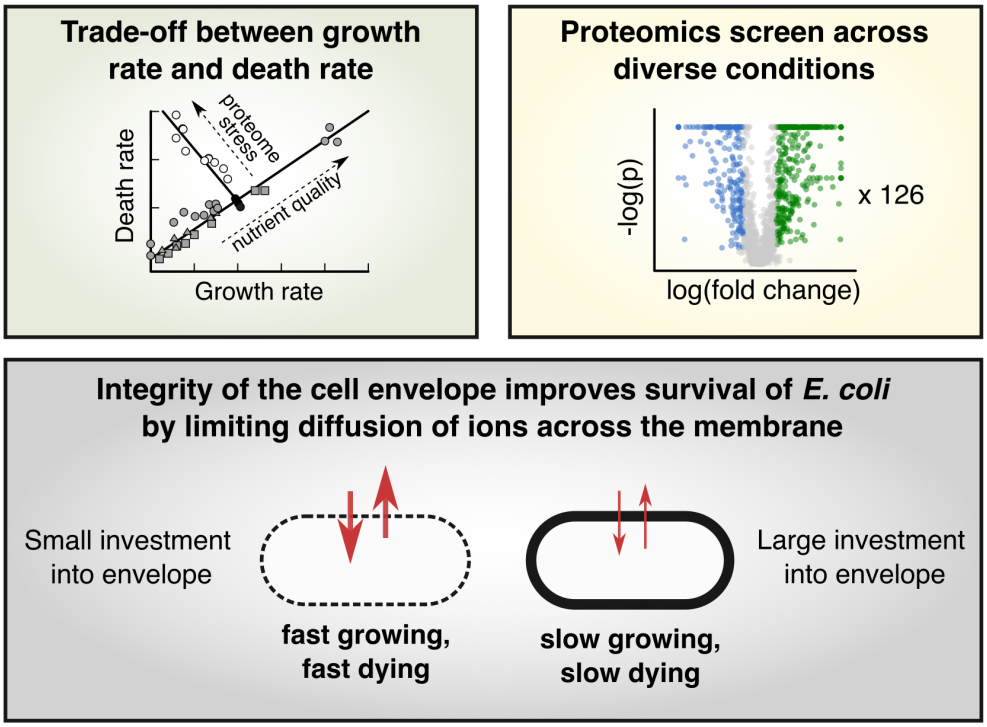

Standfirst text: A trade-off between the two major modes of bacterial lifestyle, growth and starvation can be explained by bacteria investing resources into the cell envelope to make it impermeable to ions, which improves their lifespan but comes at the expense of slowing down growth.

Highlights:

- A trade-off between growth rate and death rate confines fitness of bacteria across environments.
- Analysis of proteome signatures in 126 conditions across five independent perturbations reveals the cell envelope as a key determinant of death rate.
- The trade-off can be abolished by changing environment to a low-salt, but osmo-balanced medium where cell envelope integrity is not limiting.

Abstract

Bacteria reorganize their physiology upon entry to stationary phase. What part of this reorganization improves starvation survival is a difficult question, because the change in physiology includes a global reorganization of the proteome, envelope and metabolism of the cell. In this work, we used several trade-offs between fast growth and long survival to statistically score over 2000 *E. coli* proteins for their global correlation with death rate. The combined ranking allowed us to narrow down the set of proteins that positively correlate with survival and validate the causal role of a subset of proteins. Remarkably, we found that important survival genes are related to the cell envelope, i.e., periplasm and outer membrane, because maintenance of envelope integrity of *E. coli* plays a crucial role during starvation. Our results uncover a new protective feature of the outer membrane that adds to the growing evidence that the outer membrane is not only a barrier that prevents abiotic substances from reaching the cytoplasm, but essential for bacterial proliferation and survival.

Introduction

Nutrient limitation is a defining part of the lifecycle of microorganisms. In the absence of external nutrients, the only energy source for heterotrophic organisms is either internal storage (Fung and Kwong, 2013; Hengge-Aronis and Fischer, 1992; Strange, 1968) or nutrients retrieved by recycling dead biomass (Steinhaus and Birkeland, 1939; Zambrano and Kolter, 1996; Schink et al., 2019; Finkel, 2006). These finite energy sources can be temporarily used to maintain the cell, but will eventually deplete, exposing cells to a slow deterioration process driven by entropic forces. It was previously shown that the survival kinetics during starvation, i.e. how many cells will be still alive after a certain time, is determined by the consumption rate of these nutrients, called the maintenance rate, and the availability of nutrients (Schink et al., 2019). Because maintenance rate is a major determinant of bacterial lifespan, we expect bacteria to minimize their maintenance cost to maximize fitness in starvation.

But what determines how much maintenance bacteria need to perform, and how they can reduce it is still largely unclear. The question of maintenance is particularly puzzling, because sporulating organisms can minimize the number of active processes without losing their viability. The maintenance rate of non-sporulating bacteria is similarly not an engraved biophysical constant. Instead, *Escherichia coli,* for example, can decrease its maintenance rate and death rate over 5-fold in response to environmental cues sensed during the prior growth phase (Biselli et al., 2020).

But identifying the part of the adaptation that determines lifespan is tricky as the bacteria globally reorganize their proteome (Hui et al., 2015; Schmidt et al., 2016), macromolecular composition (Bremer and Dennis, 2008; Schaechter et al., 1958) and even morphology (Schaechter et al., 1958), when nutrients get depleted and growth slows down. This means that most properties of bacteria correlate or anti-correlate with lifespan. In addition, while several regulators and genes have been identified that react to nutrient depletion and are essential for survival, such as the general stress response regulator *rpoS* (Hengge-Aronis and Fischer, 1992), cAMP-Crp (Makman and Sutherland, 1965; Notley-McRobb et al., 1997), stringent response (Magnusson et al., 2003; Irving et al., 2021) or DNA protection in starvation *dps* (Almirón et al., 1992), there is no evidence that these systems are the limiting factors for survival.

In this paper, we analyzed diverse growth conditions and find that they heavily influence lifespan after nutrients run out. Due to the diversity in proteomic responses, we can use this information to narrow down the set of proteins that correlate with better survival and validate which parts of the adaptation determine lifespan of *E. coli* in starvation.

Results

Proteome analysis identifies proteins and processes that correlate with long lifespan

We studied *Escherichia coli* K-12, first grown in single carbon source N^+C^+ minimal medium, followed by a wash and resuspension in medium with the carbon source missing. The washing step introduces bacteria suddenly to starvation and prevents their complete adaptation. As a result, during the ensuing starvation, viability decreases exponentially (Phaiboun et al., 2015; Schink et al., 2019), with death rate depending on the previous growth condition. *E. coli* grown on carbon substrates supporting faster growth die faster than those on poor carbon substrates (Biselli et al., 2020), see Fig. 1A ('blue'). Alternatively, letting *E. coli* adapt to stationary phase on glucose minimal medium results in a death rate similar to sudden starvation from very low growth rates (Fig. 1A, open symbols placed at growth rate zero). We suspected that changes in the proteome composition, which is known to vary highly across growth conditions (Hui et al., 2015; Schmidt et al., 2016), are at least partially responsible for the observed changes in death rate. However, in a single growth perturbation, such as varying the carbon substrates, over half of all proteins were up- or downregulated (Hui et al., 2015; Schmidt et al., 2016), making it impossible to pinpoint individual proteins or processes as being responsible.

To narrow down the search for the proteins that determine lifespan, we decided to use additional growth conditions that show different changes in proteome. We identified a total of six independent perturbations, which we collectively call 'CARLOS conditions' that affect proteome composition during growth and death rate after washing and resuspension in carbon-free medium. Among these, those that reflect a change in nutrient availability (C: catabolic limitation, A: anabolic limitation, L: rich media (LB) and S: stationary phase) collapse onto a single exponential increase of death rate with growth rate, while conditions that perturb the proteome by expression of excess proteins (R: ribosome limitation, O: LacZ overexpression) fall onto an orthogonal exponential increase (Fig. 1A).

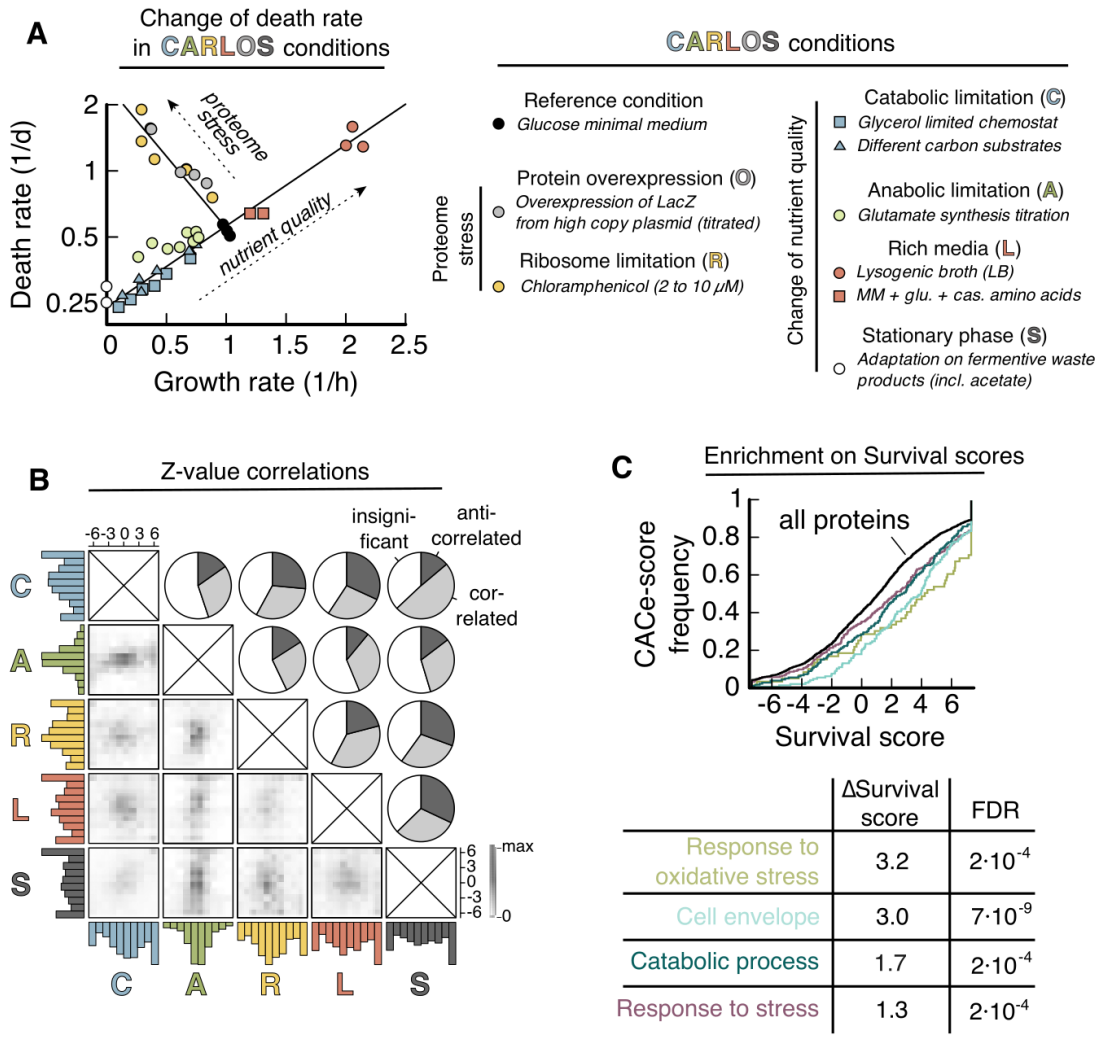

	ΔSurvival score	FDR
Response to oxidative stress	3.2	$2{\cdot}10^{-4}$
Cell envelope	3.0	$7{\cdot}10^{-9}$
Catabolic process	1.7	$2{\cdot}10^{-4}$
Response to stress	1.3	$2{\cdot}10^{-4}$

Figure 1 Proteome composition and death rates in CARLOS conditions.

(**A**) Death rate versus pre-starvation growth rate on a semilog-plot. CARLOS conditions are defined in legend. CARLOS conditions that perturb nutrient quality (C, A, L and S) lead to an exponential increase of death rate. Conditions that stress the proteome (R and O) show an orthogonal exponential increase with slower growth. Each data point is a single experiment. Chemostat (C) and parts of (L) are from Ref. (Biselli et al., 2020). See Table S1 for data.

(**B**) Pair-wise comparison of protein Z-values between conditions. Histograms of Z-values of individual conditions (colored) and grey values of the 2D histogram between pairs of conditions are normalized to their respective maximum value. The fraction of proteins that correlate, anti-correlate or are insignificant is calculated by thresholding in the 2D histogram, see Fig. EV1A for an illustration.

(**C**) Z-values are merged into a single 'Survival score' for each protein that measures correlation of abundance with survival across all experiments. A detailed description of the construction of the score is given in Box 1. Several GO-processes are significantly enriched (FDR levels of the Benjamini-Hochberg step-up procedure) towards higher scores. ΔSurvival score is calculated as the difference in median Survival score between a process and the background of all proteins.

CARLOS conditions result in substantial changes in proteome composition. We analyzed these changes in the proteome using published proteomics data from three different repositories (Data ref: Houser et al., 2015; Data ref: Hui et al., 2015; Data ref: Schmidt et al., 2016), which individually cover a subset of the CARLOS conditions (C, L & S in (Data ref: Schmidt et al., 2016), C, A & R in (Data ref: Hui et al., 2015) and S in (Data ref: Houser et al., 2015)). To be able to compare proteins across conditions and across data sets, we created a composite statistical score, termed “Survival Score", explained in detail in Box 1 and the Methods section.

In short, we compare protein abundance levels between data sets and assign a positive score (in the form of a Z-value), if the protein is correlated with better survival and a negative score if the protein is anticorrelated (Box 1, step 1). We collect these scores over the variety of conditions and data sets and iteratively merge the scores, while correcting for statistical dependencies and ignoring missing values (steps 2-4).

Z-values calculated from individual data sets of similar perturbations or different sources (Box 1, step 2) are highly correlated (Fig. EV1A&B) and are used to create merged Z-values for each protein (Fig. EV1C & Box 1, step 3). Histograms of these merged Z-values on the condition level (step 3) are shown as colored 1D histograms in Fig. 1B, normalized to the highest value. We had to exclude ‘O, LacZ overexpression’ from this analysis due to lack of sufficient statistical data, shortening CARLOS to CARLS, but we will integrate qualitative information from this condition below.

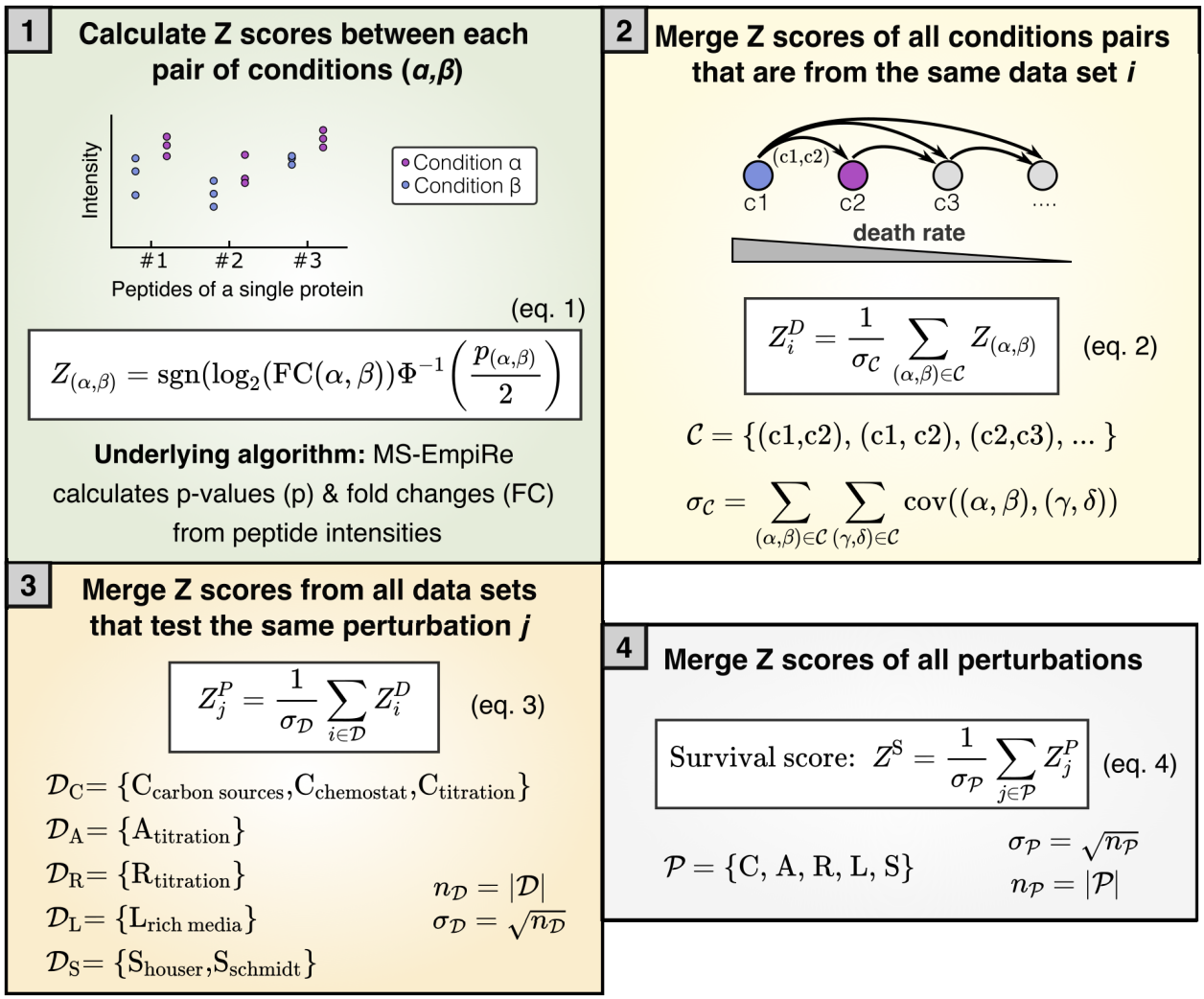

Box 1. Calculation of Survival scores from multi-condition proteomics data sets. The survival scores Z^S quantifies how well a protein correlates with lifespan over all CARLS perturbations and is calculated in the steps listed below. Jupyter Notebooks implementing the procedure below are provided in the SI (see also data availability section).

1) Using the MS-Empire statistical software package, we calculated p-values and fold-changes (FC) of proteins between a pair of conditions (α, β) based on the underlying peptide intensities across replicates (blue, purple). We use this information to calculate the Z score of a pair of conditions, $Z_{(\alpha,\beta)}$, in eq. (1) using the direction of the fold-change, where 'sgn' is the sign function, and the significance of the regulation, using the inverse cumulative standard normal distribution function Φ^{-1}.
2) Next, we merge all $Z_{(\alpha,\beta)}$ that are from the same data set $\mathcal{C}$, into a new Z value of a data set Z_i^D in eq. (2), where the subscript i stands for the specific data set. An example of a data set are $Z_{(\alpha,\beta)}$ scores of different carbon sources derived from the same data repository. The pairs of conditions (α, β) are sorted from high to low death rate, such that a positive Z-value corresponds to correlation with lower death rate. Because the merged score Z_i^D should

follow a standard normal distribution with standard deviation of 1, merging $Z_{(\alpha,\beta)}$ scores requires normalization by the standard deviation across the whole data set, $\sigma_{\mathcal{C}}$. The standard deviation can be derived from the covariance matrix, where $\mathrm{cov}\big((\alpha,\beta),(\gamma,\delta)\big)$ is 1 if $(\alpha = \gamma \text{ AND } \beta = \delta)$, 0.5 if $(\alpha = \gamma \text{ XOR } \beta = \delta)$ and 0 otherwise (Ammar et al., 2019).

3) Next, we merge all Z_i^{D} that belong to the same perturbation into a single score for each perturbation Z_j^{P}, where the subscript j stands for any of the CARLS conditions. Because data sets are independent of each other, the standard deviation $\sigma_{\mathcal{D}}$ depends only on the number of data sets $n_{\mathcal{D}}$. For A, R and L there is only a single data set, such that $Z_j^{\mathrm{P}} = Z_i^{\mathrm{D}}$. Fig. EV1 visualizes this merging step for C and S conditions.

4) Finally, all Z_j^{P} are merged into a single Z^{S}, which we call 'Survival score'. As in panel 3, the standard deviation $\sigma_{\mathcal{P}}$ depends only on the number of perturbations $n_{\mathcal{P}}$ that are measured.

Next, we compared Z-values of the conditions in a pair-wise manner by plotting 2D histograms of Z-values detected in both respective conditions (Fig. 1B, bottom left of matrix). By classifying proteins that score above $|Z| > 1.28$, which corresponds to $p < 0.1$, as significantly correlated or anti-correlated, depending on the direction, we confirmed that proteome changes across different conditions are partially orthogonal to each other (Fig. 1B, top right of matrix). This means that each condition has additional information that can help us narrow down the target set of proteins. Finally, we merged Z-values of the individual CARLS conditions into a single 'Survival score' that measures the global correlation strength of proteins with lifespan (Box 1 step 4). The resulting list of CARLS Z-values and 'Survival scores' for over 2000 proteins is available in Table S2.

Fractions of the proteome determining death rate can be either beneficial or harmful. To understand which of these fractions is dominant, we used the 'O' condition, where overexpression of a useless protein leads to a decrease in the abundance of virtually all proteins simultaneously (Fig. EV2). This condition led to a 5-fold increase in death rate (Fig. 1A, gray symbols), as we would expect for largely beneficial proteins determining death rate. Thus, we restricted our further analysis to positive Survival scores, where a higher abundance correlates with longer lifespan across conditions.

Finally, we used Survival scores of all proteins measured in at least 3 of the 5 CARLS conditions to identify gene ontology (GO) processes and cellular compartments that contain proteins with significantly larger Survival scores than average. Using a Kolmogorov-Smirnov test, we evaluated enrichment of proteins in GO-processes and compartments, which includes 'oxidative stress response', 'response to stress', 'catabolic process' and 'cell envelope' as some of the highest

192 scoring GO-processes (Fig. 1C, see Table S3 for full list). Note that GO-processes are not mutually
193 exclusive and can contain the same proteins, which is particularly true for 'oxidative stress
194 response', which substantially overlaps with 'response to stress'.
195
196 *Death rate depends on the integrity of the cell envelope*
197 We next wanted to test if any of these processes/compartments causally affect bacterial lifespan.
198 The response to oxidative stress had the highest Survival score in our analysis, with proteins such
199 as catalases KatE (Survival score: 7.3) and KatG (7.3), superoxide dismutase sodA (6.5), and
200 hydroperoxidase AhpC (6.2), all of which are essential to *E. coli's* adaptation to stress (Farr et al.,
201 1988; Farr and Kogoma, 1991; Dukan and Nyström, 1999; Chiang and Schellhorn, 2012),
202 correlating well with survival across CARLOS conditions. Therefore, we first tested whether
203 oxidative stress limits lifespan of starving bacteria by starving bacteria in anaerobic conditions,
204 where oxidative damage should be absent. It was previously reported that starved *E. coli* suffer
205 from protein carbonylation and that anaerobic conditions can prevent carbonylation and stop death
206 (Dukan and Nyström, 1999). However, to our surprise, our results showed the opposite. We found
207 that death in anaerobic conditions was even faster than in aerobic conditions (Fig. EV3A). This
208 did not depend on whether growth prior to starvation was in aerobic or anaerobic conditions.
209 Similarly, adding antioxidants glutathione, ascorbic acid or mercaptoethanol, which could prevent
210 carbonylation during starvation, did not decrease the death rate of starvation *E. coli* (Fig. EV3B).
211
212 Also, inducing the 'response to stress' did not decrease death rate, despite the high score. Neither
213 inducing its expression using heat shocks, low pH nor high osmolarity during growth, all of which
214 significantly increase abundance of 'response to stress' proteins (Fig. EV4A-C), resulted in
215 changes of death rate of *E. coli* in reference starvation conditions (Fig. EV4D). One possible
216 explanation is that our wild-type strain NCM3722 is insensitive because one of the master
217 regulators of the stress response, *rpoS*, contains a premature amber stop codon, which reduces
218 expression of *rpoS* dependent genes (Mori et al., 2021). But restoring *rpoS* did not decrease death
219 rate (Fig. EV4E). In contrast, knockouts of *rpoS* still showed significantly increased death rates
220 compared to NCM3722 (Fig. EV4E), which indicates that the *rpoS* gene is sufficiently functional
221 in our strain. Only a knock-out *rssB,* a gene responsible for degradation of RpoS (Muffler et al.,
222 1996) lead to a significant decrease in death rate (Fig. EV4E), similar to previous reports (Fontaine

223 et al., 2008). These conflicting observations warrant further investigation into physiological role
224 of *rpoS* and *rssB* in starvation survival. However, it is known that *rpoS* knockouts do not remove
225 the growth-death dependence in carbon limitation (Biselli et al., 2020) that forms the basis of our
226 analysis.
227
228 Another high-scoring class of proteins identified by our analysis were proteins of the cell envelope,
229 which includes the periplasm, cell wall and outer membrane (Fig. EV5 for graphical summary).
230 Proteins associated with the cell envelope make up about 13% of the proteome in rich nutrient
231 conditions, and up to 23% for bacteria adapted to stationary phase (Fig. 2A and Table S4). In
232 addition to the GO analysis, we also noticed the cell envelope in a knock-out screen of high-scoring,
233 non-essential genes. The fastest dying knock-out in the screen, Δ*lpp,* encoded a protein located in
234 the cell envelope (Table S5). In contrast, knockouts of most other genes, especially those belonging
235 to stress response and oxidative damage, had little or no impact of death rates in starvation (Table
236 S5), further corroborating that many of them are non-limiting in our conditions.
237
238 The physiological role of Lpp (Survival score: 7.2), together with OmpA (5.8), is to physically
239 link outer membrane and cell wall. These proteins are essential for the cell envelope's mechanical
240 integrity and make up around half the cell envelope proteome and up to 12% of the total proteome
241 (Fig. 2A). Motivated by this finding, we tested more cell envelope proteins, independent of their
242 Survival scores, and found that starvation-survival is highly sensitive to knock-outs across
243 different functionalities of the cell envelope (Fig. 2B), from outer membrane protein folding
244 (BamE & Skp), cell wall synthesis and modification (Prc, NlpI, DolP & NlpD), phospholipid
245 recycling (MlaA & MlaC) to cell envelope regulators (CpxA & RseA).
246

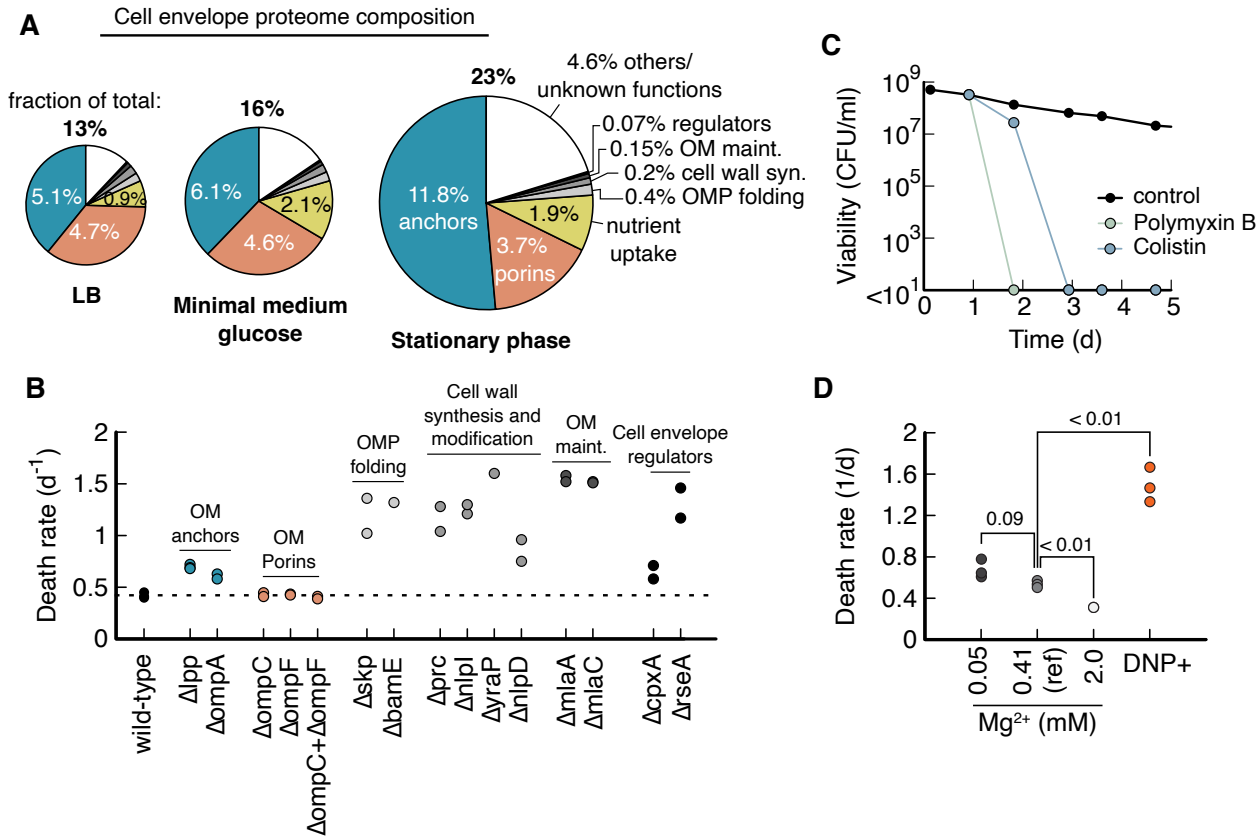

Figure 2 Cell envelope integrity plays a major role in starvation survival.

(**A**) Proteome composition of the cell envelope (see Fig. EV5 for details on the cell envelope structure) for cultures during exponential growth on LB, glucose minimal medium and stationary phase. Size of pie indicates fraction of total proteome that is associated with envelope. Outer membrane anchors (Lpp and OmpA) constitute half of the cell envelope proteome. Major porins (OmpC and OmpF) and nutrient uptake (large number of binding proteins) constitute other major fractions. Quantification of abundancies are in Table S4 using data from Ref. (Data ref: Schmidt et al., 2016).

(**B**) Knock-out of several genes with different functionalities in the cell envelope increase death rates. Growth in glycerol minimal medium, starvation induced by glycerol depletion.

(**C**) 8 μg/ml Polymyxin B and 4 μg/ml Colistin, added daily to cultures previously grown on glucose minimal medium (reference condition) with the first dose at 24h. Antibiotic concentration was 10x minimum inhibition concentration during growth (MIC). Each data point is the average of two biological repeats. Error bars are not shown because the variation is smaller than symbol size. Viabilities indicated at $<10^1$ mean no colonies were detected from 100 μl culture.

(**D**) Death rates for different Mg^{2+} concentrations. Reference condition (black circle in Fig. 1A) has 0.41 mM Mg^{2+}. DNP+ cultures were supplemented with 1 mM 2,4-dinitrophenol during starvation in reference medium. Each data point is from a single experiment. All cultures were grown in glucose minimal medium. P-values (Student's t-test, two-tailed) are indicated in comparison to the reference condition.

268 Conversely, only knockouts of porins, which facilitate diffusion of biomolecules across the outer
269 membrane, have high Survival scores, and are highly abundant (Fig. 2A), did not change death
270 rate (Fig. 2B).
271
272 This sheer abundance of cell envelope proteome makes it a compelling candidate for determining
273 death rate in carbon starvation, as it would mean adaptation to optimal starvation survival would
274 require a major reorganization of the proteome, rather than simply synthesizing a small set of
275 proteins that could be achieved with a limited amount of stored nutrients. This could explain why
276 the prior growth condition has such a big influence on starvation survival.
277
278 Many of the knock-outs that we identified are known to impair the mechanical integrity of the cell
279 envelope (Bryant et al., 2020; Malinverni and Silhavy, 2009; McBroom et al., 2006; Rojas et al.,
280 2018; Schäfer et al., 1999; Suzuki et al., 1978; Tsang et al., 2017; Yem and Wu, 1978). Therefore,
281 we hypothesized that the mechanical integrity of the cell envelope plays a role in survival. To test
282 this hypothesis, we applied antibiotics that are known to compromise the cell envelope, polymyxin
283 B and colistin. Both antibiotics were highly effective when added 24 h into starvation, killing the
284 entire population within 24 h and 48h, respectively (Fig. 2C). This is unusual, as most other
285 antibiotics are ineffective on starving bacteria (Nguyen et al., 2011; Schink et al., 2022).
286 Polymyxin B and colistin insert into the outer membrane between lipid A molecules and displace
287 Mg^{2+} ions that shield repulsive negative charges between lipid A (Moore et al., 1986). Similarly,
288 supplementing the starved culture with DNP, which acts as an ionophore and permeabilizes
289 bacteria (McLaughlin, 1972) increased death rate 2.8-fold (Fig. 2D).
290
291 These results show that cell envelope integrity is essential for survival. In addition, we wanted to
292 know if cell envelope integrity is also limiting for survival and tested the reverse effect by
293 increasing Mg^{2+} concentrations. Indeed, we found a 40% drop in death rate at high Mg^{2+}
294 concentrations compared to the reference condition (Fig. 2D), suggesting that cell envelope
295 integrity is both essential and limiting.
296
297 *Ion homeostasis and cell envelope integrity account for the variation of starvation survival*

298 But how does cell envelope integrity influence survival? We recently showed that the cost of ion
299 homeostasis is a major determinant of lifespan of bacteria in carbon starvation (Schink et al., 2022).
300 Based on this work, we hypothesize that changes in death rates in the CARLOS conditions were
301 due to changes in the cost of ion homeostasis, mediated by the envelope proteome affecting
302 membrane permeability. If membranes are less permeable, less energy is required to actively pump
303 ions across the cytoplasmic membrane to remain ion homeostasis. This reduction in maintenance
304 should then result in a lower death rate (Schink et al., 2019).
305
306 To test this hypothesis we used an 'osmo-balanced' medium with low salt concentrations, designed
307 to minimize the content of inorganic ions that can diffuse across membranes (Schink et al., 2022).
308 This medium reduces the death around 4-fold in standard glucose minimal medium conditions due
309 to a reduction in maintenance rate required for ion homeostasis (Schink et al., 2022). If changes in
310 the membrane permeability were responsible for the modulation of death rate in Fig. 1, we predict
311 that the osmo-balanced medium should remove the growth-death dependence. In a perfect scenario,
312 in which loss of ion homeostasis is the only possibility to die we would predict death rate to
313 decrease to zero for all conditions, but we already know from previous work (Schink et al., 2022)
314 that death rate does not decrease to zero with this medium, presumably because at some point
315 lifespan will be limited by other causes.
316
317 On the other hand, if the growth-death dependence is independent of permeability of ions, for
318 example if the modulated proteins and processes are preventing some type of damage or are
319 influencing nutrient recycling, then we would expect the growth-death dependence to remain in
320 'osmo-balanced' medium but be shifted to a lower death rate.
321
322 Because the osmo-balanced medium allows us to distinguish whether the growth-death relation is
323 due to a modulation of the ability to deal with ions in the medium, we grew *E. coli* in the CARLOS
324 conditions followed by washing and resuspension in 'osmo-balanced' medium. We found that the
325 characteristic growth rate dependence of the CARLOS condition was indeed abolished and no
326 significant correlation between growth rate and death rate remained (Fig. 3). This confirms that
327 differences of the cell envelope integrity and membrane permeability underlie the variations in
328 death rate seen in Fig. 1A.

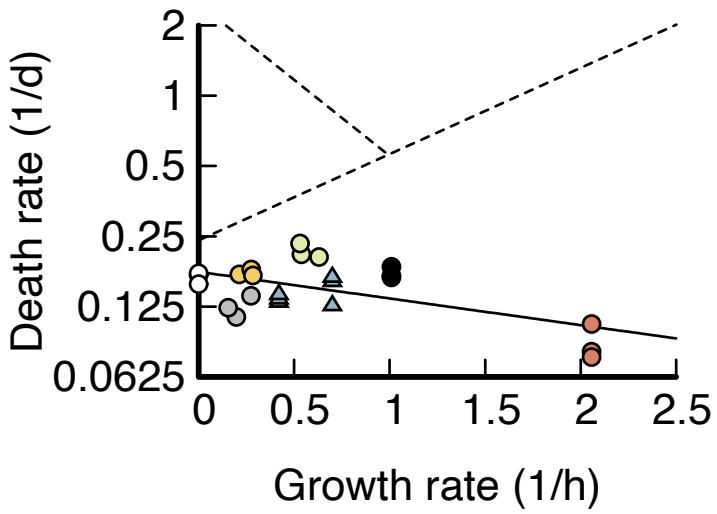

Figure 3 Death rates in osmo-balanced medium. Death rate plotted versus growth rate on a semi-log scale for experiments in 'osmo-balanced' medium. Colors indicate carbon limitation (C, 'blue', acetate and glycerol), anabolic limitation (A, 'green', 3μM IPTG), ribosome limitation (R, 'yellow', 4μM Chloramphenicol), rich medium (L, 'red', LB), LacZ overexpression (O, 'grey', 10ng/ml cTc), stationary phase (S, 'white') and the glucose reference condition ('black'), as defined in Fig. 1A. The data shows weak anti-correlation with growth rate; solid black line is an exponential fit to the data ($R^2 = 0.34$). Dashed lines are the exponential fits to the CARLOS data in Fig. 1A.

Discussion

We performed an analysis of proteomics data to identify proteins, processes and cellular compartments that contribute to improved survival of carbon starvation. We identified cell envelope proteome and the membrane permeability as a key determinant of survival.

Limitations of the study

Before discussing the implications of our work, we should spell out the limitations of our search for proteins that determine death rate. First, because we assume that the same proteins determine the modulation of death rate across all CARLOS conditions, we are prone to miss proteins that contribute to death rate in a single (or small subset) of conditions. Secondly, because we focused our analysis on the level of processes and cellular compartments, we will miss proteins and mechanisms that are not connected to significant processes and compartments. Therefore, these proteins could be undetected, even though they should in principle pop up with a high Survival-score (Table S2). It is thus possible that we missed additional mechanisms not connected to the cell envelope. Thirdly, the quality of the data sets varies across sources. The Schmidt et al data set, used for C, S and L, has a deep coverage that includes many low abundance proteins, and as a

355 result, there is large number of proteins missing values in A and R (Table S2), which are derived
356 from data sets with less coverage. This leads to some limitations in the scoring and the construction
357 of the overall survival score. In order to retain the information available in the data set, we
358 constructed our scores in such a way, that we omit missing values in the survival score, which
359 leads to larger contributions of the available scores to the overall score. This can have two opposing
360 types of effects: 1) Globally correlating proteins that are only measured in a subset of perturbations
361 (which are generally of lower abundance) will have lower overall score, which introduces a bias
362 towards proteins of high abundance. 2) If a protein has a strong anti-correlation in one of the missed
363 conditions, the estimated survival score will be higher than it should be. To mitigate the effects of
364 this in the downstream analysis, we perform our final enrichment analysis on the subset of proteins
365 that were measured in at least 3 of the 5 CARLS conditions. In addition, proteins can be present
366 in the data, but measured with so much underlying noise, that the direction of regulation cannot be
367 determined with high confidence. This results in low Z-values and the effects are like the effects
368 of missing values mentioned above. Finally, the number of individual data sets for each
369 perturbations varies. While we compensate the impact of the number of data sets on the final
370 Survival score by weighing the scores appropriately, more data sets per perturbation will reduce
371 noise and improve the scoring. This creates a bias towards perturbations with many data sets, such
372 as C, at the expense of those with few, such as A and R. It should be noted that the challenges of
373 missing values, bias towards higher abundant proteins and measurement noise are common in the
374 analysis of proteomics data and we have strived to find a compromise between stringency and
375 comprehensiveness in the construction of our score.
376
377 Nevertheless, we have presented a variety of results that allow us to be confident in our main
378 conclusions. In the construction of our score, we have shown good correlation between identical
379 types of perturbations on independent data sets (Fig. EV1). We see enrichment in a canonical set
380 of processes (Fig. 1C) and an increase in death rate for knockout of key genes in the cell envelope
381 (Fig. 2B). We additionally validated that both weakening and strengthening the cell envelope affect
382 death rate (Fig. 2C) and established that the growth-death relation can be abolished in the absence
383 of ions in the medium (Fig. 3), which is a strong indication that the mechanism identified by our
384 analysis, i.e., the integrity of the cell envelope, is the major contribution to the growth-death
385 dependence of Fig. 1.

386

387 *Cost of building a strong cell envelope*

388 Building a strong cell envelope is a costly endeavor. A third of the dry weight of a typical cell
389 consists of cell envelope biomass, half of which consists of protein, and the other half
390 phospholipids, LPS and cell wall (Neidhardt, 1996). Given the substantial fraction of biomass
391 devoted to the cell envelope, it is reasonable that bacteria reduce this biomass investment into the
392 cell envelope in favorable growth conditions, and instead focus on maximizing their growth rate.
393 However, because of the magnitude of the biomass investment into the cell envelope, bacteria
394 cannot easily adapt to starvation using carbon stores after sudden nutrient depletion, which would
395 explain why pre-growth conditions have such a big effect on starvation survival, and why optimal
396 survival requires prolonged adaptation.

397

398 *Role of the outer membrane in cell envelope integrity and starvation survival*

399 Surprisingly, many of the proteins that we found to affect survival rates in carbon starvation are
400 related to the outer membrane and overall, our data demonstrates an important role of the outer
401 membrane for starvation survival. While the outer membrane is known to be a permeability layer,
402 e.g., to antibiotics, it is less clear how it could achieve a similar effect for inorganic ions, which
403 would explain improved survival in starvation. Ion export pumps, such as NhaA, are thought to
404 only span the cytoplasmic membrane, meaning that ion gradients across the outer membrane
405 should equilibrate. In this case, the outer membrane should offer little protection from inorganic
406 ions. Indeed, in 'plasmolysis' from osmotic shocks, the inner membrane contracts as a result of
407 osmotic pressure, while the outer membrane largely maintains its shape (Rojas et al., 2018),
408 indicating that osmolytes readily diffuse into the periplasm. There is, however, considerable
409 biochemical and mechanical interplay between inner and outer membrane that could contribute to
410 permeability changes. Both membranes share phospholipids, and the outer membrane is involved
411 in recycling lipids that have accumulated on the outer leaflet of the outer membrane (Malinverni
412 and Silhavy, 2009). Recently, the outer membrane has been found to mechanically stabilize the
413 inner membrane, e.g., via the tol-pal system, which is essential for bacteria to reach plasmolysis
414 in starvation (Rojas et al., 2018; Shi et al., 2021). Integrity of the cell envelope could also protect
415 periplasmic proteins from damage. We therefore argue that a mechanically strong cell envelope

416 allows Gram-negative bacteria to stabilize and protect its cytoplasmic membrane, allowing
417 bacteria to reduce their maintenance cost and increase their lifespan.
418
419 **Materials and Methods**
420 *Strains*
421 All strains used in this study are derived from wild type *E. coli* K-12 strain NCM3722 (Soupene
422 et al., 2003). Strains NQ381 (attB:Plac-xylR, Km-Pu-lacY) was used for 'catabolic limitation' and
423 was described in Ref. (You et al., 2013). In NQ381 strain the expression of the lactose transporter
424 lacY is induced using 3-Methoxybenzamide (3MBA). NQ393 (ΔgdhA+plac-gltBD,
425 attB(phage):lacIQ-tetR::Sp, ΔlacY) was used for 'anabolic limitation' and is described in Ref. (Hui
426 et al., 2015). Using isopropylthio-β-galactoside (IPTG), the expression of gltBD is induced, which
427 encodes glutamate synthase. NQ1389 (Ptet-tetR on pZA31; Ptetstab-lacZ on pZE1) was used to
428 overexpress LacZ using chlortetracycline (cTc) as inducer and is reported in Ref. (Basan et al.,
429 2015a). All knockouts shown in Fig. 2 were transferred from the Keio collection (Baba et al., 2006)
430 to NCM3722 via P1 transduction to yield strain. Knockouts from Table S5 are taken from the Keio
431 collection (Baba et al., 2006) and compared to the ancestor wild-type BW25113.
432
433 *Culture medium*
434 The culture medium "$N^{-}C^{-}$ minimal medium" (Csonka et al., 1994), contains 1g K2SO4, 17.7 g
435 K2HPO4, 4.7 g KH2PO4, 0.1 g MgSO4·7H2O and 2.5 g NaCl per liter. The medium was
436 supplemented with 20 mM NH4Cl, as nitrogen source, and varying carbon sources. The 'reference
437 glucose condition' contained 0.2% glucose. All chemicals were purchased from Sigma Aldrich,
438 St. Louis, Mo, USA. The 'osmo-balanced' medium is described in (Schink et al., 2019), and
439 contains 0.2 M MOPS (3-(N-morpholino)propanesulfonic acid), titrated to pH 7 with KOH, and 1
440 mM $MgCl_2$, 0.1 mM $CaCl_2$, 0.16 mM K_2SO_4, 0.5 mM K_2HPO_4, 22mM NH_4Cl and lacks a carbon
441 source. Cultures starved in the 'osmo-balanced' medium were previously grown in N-C- medium
442 supplemented with NH_4Cl and glucose.
443
444 *Culture conditions*
445 Prior to each experiment, bacteria were streaked out from -80ºC glycerol stock on an LB agar plate
446 supplemented with antibiotics if necessary. Bacteria were cultured in three steps. First, a seed

447 culture was grown in lysogenic broth (LB) from a single colony. Second, the seed culture was
448 diluted in $N^{-}C^{-}$ minimal medium supplemented with 20 mM NH_4Cl and a carbon source and
449 grown overnight for at least 5 doublings to exponential phase. The next morning, the overnight
450 culture was diluted into fresh, pre-warmed $N^{-}C^{-}$ minimal medium supplemented with 20 mM
451 NH_4Cl and a carbon source and grown for another 5 to 10 doublings. At an optical density of 0.5
452 or below, the culture was washed by centrifugation (3 min at 3000 g) and resuspension into fresh,
453 carbon-free, pre-warmed $N^{-}C^{-}$ minimal medium supplemented with 20 mM NH_4Cl. This
454 washing step removes excreted byproducts such as Acetate. For growth conditions known to fully
455 respire carbon, e.g. wild-type NCM3722 grown on glycerol (Basan et al., 2015b), this washing
456 step was omitted.
457
458 NQ381 was grown overnight and during the experimental culture with the inducer concentrations
459 indicated in Table S1. NQ1389 was grown without inducer overnight, with indicated inducers
460 added after dilution of the overnight culture, to prevent escape mutations and plasmid loss. NQ399
461 was grown with 100 μM IPTG overnight and the indicated IPTG concentrations after dilution of
462 the overnight culture.
463
464 For culturing we used 20 mm x 150 mm glass test tubes (Fisher Scientific, Hampton, NH, USA)
465 with disposable, polypropylene Kim-Kap closures (Kimble Chase, Vineland, NJ, USA) filled with
466 5 to 7 ml of medium. Cultures were sealed with Parafilm "M" (Bemis Company, Neenah, WI,
467 USA) to prevent evaporation.
468
469 *Death rate measurements*
470 Death rates were extracted using a linear fit of log-transformed viability measurements during the
471 first 10 days of starvation, or until the viability reached below 10^7 CFU/ml, whichever came first.
472 Note that after the initial, exponential phase of starvation that we study, mutants take over, viability
473 stabilizes, and cultures enter 'long-term stationary phase'. For viability measurements, cultures
474 were diluted in untreated, sterile 96 well plates (Celltreat, Pepperell, MA, USA) in three to four
475 steps using a multichannel pipette (Sartorius, Göttingen, Germany) to a target cell density of about
476 4000 CFU/ml. 100 μl of the diluted culture was spread on LB agar plates supplemented with 25
477 μg/ml of 2,3,5-triphenyltetrazolium chloride to stain colonies bright red using Rattler Plating

478 Beads (Zymo Research, Irvine, CA, USA), and incubated for 12 to 24 hours. Images of agar plates
479 were taken with a Canon EOS Rebel T3i (Tokyo, Japan) mounted over an LED light box 'Lightpad
480 A920' (Artograph, Delano, MN, USA), and analyzed using a custom script in Cell Profiler
481 (Carpenter et al., 2006). Colony forming units per volume (CFU/ml) were calculated by
482 multiplying the number of colonies per agar plate by the dilution factor.
483
484 *Stress conditioning*
485 For pre-stressing, wild-type *E. coli* NCM3722 was grown in glucose minimal medium, either in a
486 water bath at 40ºC ('heat stress'), in medium supplemented with 50 mM NaCl ('osmotic stress')
487 or in $N^{-}C^{-}$ medium adjusted to pH 6 using KOH ('pH stress'). At an optical density $OD6_{00}$ of
488 about 0.5, cultures were washed and transferred to pre-warmed, carbon-free $N^{-}C^{-}$ supplemented
489 with 20 mM NH_4Cl, and the decay of viability was recorded for about 10 days.
490
491 *Anaerobic culturing*
492 For anaerobic growth and starvation, cultures were grown in 0.05% glucose minimal medium in a
493 vinyl anaerobic chamber (COY Lab Products, Grass Lake, Mi, USA), in Erlenmeyer flasks
494 (Chemglass, Vineland, NJ, USA) on a magnetic stirrer (IKA RO10, Staufen, Germany), and not
495 washed after the end of growth. For aerobic growth and anaerobic starvation, cultures were grown
496 in 0.05% glucose minimal medium in an air incubator. At an optical density of about 0.5, cultures
497 were centrifuged, supernatants were discarded, and pellets were introduced to the anaerobic
498 chamber. In the anaerobic chamber, pellets were resuspended in pre-warmed, carbon-free minimal
499 medium. All media were degassed prior to being introduced to the anaerobic chamber and left with
500 open lid to be equilibrated for one week.
501
502 *Proteomics data processing*
503 The MS proteomics data was downloaded from the corresponding PRIDE partner repositories
504 (Schmidt et al.: PXD000498, Hui et al.: PXD001467, Houser et al.: PXD002140). For the Schmidt
505 and Houser data sets, the .raw files were downloaded, for the Hui data set, peptide-intensity
506 mappings were downloaded. The Schmidt and Hui data sets were searched MaxQuant (Cox and
507 Mann, 2008) v. 1.5.7.4 using standard settings and "Label Free Quantification" (LFQ) and "Match

508 between runs". The Schmidt and the Houser data sets were searched against the reviewed Uniprot
509 *E. coli* database (03/2019).
510
511 *Differential expression analysis of proteomics data*
512 All data sets were processed with the MS-EmpiRe (Ammar et al., 2019) algorithm for differential
513 quantification, which assigned fold changes and significance scores to each protein in a condition
514 pair. For the Schmidt and Houser data sets, the MaxQuant "peptides.txt" and "proteinGroups.txt"
515 files were used as input. The Hui data set was pre-processed as follows: As in the experimental
516 setup of Hui et al. the data was quantified relative to a ^{15}N-labelled spike-in, a direct assessment
517 of LFQ values was not optimal. Similar to the approach of Ref. (Geiger et al., 2010), we first
518 assessed the fold changes of each peptide relative to its heavy labeled spike-in. To preserve the
519 intensity information, we re-scaled each spike-in fold change by the median intensity of the spike-
520 in peptide over all conditions. This resulted in pseudo-intensities, which we further processed in a
521 "LFQ-like" manner using MS-EmpiRe.
522
523 *Z-value based ranking of the proteome perturbations*
524 As displayed in Fig. 1 and discussed in the main text, each growth condition has a corresponding
525 death rate. Additionally, when we compare two conditions with one condition having a lower death
526 rate than the other, we expect the lower death rate to be caused by increased expression of proteins.
527 In our ranking, we hence had to identify proteins that show increased expression for decreased
528 death rate over all conditions.
529
530 Our initial data set consisted of "Transporter Titration" (C), "Ribosome Limitation" (R) and
531 "Anabolic Limitation" (A) in the Hui set, "Carbon Substrates" (C), "Chemostat" (C), "Rich Media"
532 (L), "Stationary Phase" (S), "Osmotic Shock", "Heat Stress" and "PH Stress" in the Schmidt set
533 and "Stationary Phase" (S) in the Houser set. Each data set had a glucose reference condition.
534
535 The "Stationary Phase", "Osmotic Shock", "Heat Stress" and "PH Stress" perturbations were
536 compared to the corresponding glucose reference using differential expression analysis with MS-
537 EmpiRe. This assigned to each protein a log fold change denoting the change in expression and a
538 significance score denoting the confidence in an expression change. The remaining perturbations

539 were compared differently, because they consisted of multiple experiments with varying
540 perturbation strength, e.g. different levels of transporter titration in the "Transporter Titration" data
541 set. The individual conditions within a data set were ranked by their corresponding death rate and
542 all combinations were compared in an increasing manner (e.g. c1 vs c2, c2 vs c3, c1 vs c3). This
543 way, positive fold changes always correlate with better survival.
544
545 Concerning the Survival score calculation, our data was structured as follows: We have the five
546 different CARLS perturbations, which we denote here as the set of perturbations $\mathcal{P}$. Each of the
547 perturbations in $\mathcal{P}$ has one or more data sets $\mathcal{D}$, which are measurements of this perturbation type.
548 For example, there are three data sets that belong to the perturbation of type C: different carbon
549 sources (Data ref: Schmidt et al., 2016), the chemostat data set (Data ref: Schmidt et al., 2016),
550 and the data set, where carbon uptake was regulated by transporter titration (Data ref: Hui et al.,
551 2015). In other words, $\mathcal{D}_C = \{\mathcal{C}_{\text{carbon sources}}, \mathcal{C}_{\text{chemostat}}, \mathcal{C}_{\text{titration}}\}$, where $\mathcal{C}$ is the respective set
552 of condition pairs. A condition pair (α, β) is the comparison of a condition α (e.g. glucose) against
553 another condition β (e.g. acetate).
554
555 We started the calculation of the score at the level of a single condition pair and the score is
556 calculated separately for each individual protein X. First, Box 1, step 1, we applied a Z-value
557 transformation to a each condition pair (α, β) of protein X as follows:

$$Z_{(\alpha,\beta)} = \text{sgn}(\text{log2FC}(\alpha, \beta)) \left|\phi^{-1}\left(\frac{p_{(\alpha,\beta)}}{2}\right)\right| \qquad \text{(eq. 1)}$$

558 where log2FC is the log2 transformed fold change, p the p-value determined by MS-EmpiRe, sgn
559 is the sign function and ϕ^{-1} is the inverse cumulative standard normal distribution function. The
560 Z-value $Z_{(\alpha,\beta)}$ is the distance from zero in a standard normal distribution and can immediately be
561 transformed back into a significance score. The higher the absolute value of the Z-value is, the
562 more significant a measurement is. The Z-value carries both the direction of a regulation (via its
563 sign) and its significance (via its value).
564
565 Next, Box 1, step 2, we merged the set of all condition pairs $\mathcal{C}$ which belonged to the same data
566 set D via the formula:

$$Z_i^D = \frac{1}{\sigma_{\mathcal{C}}} \sum_{(\alpha,\beta)\in\mathcal{C}} Z_{(\alpha,\beta)} \qquad \text{(eq. 2)}$$

where Z_i^D corresponds to the normalized Z value of the i-th data set. Normalization was performed by dividing by the standard deviation of the summed random variables denoted as $\sigma_{\mathcal{C}}$, which is the square root of the variance.

Generally, the variance of the sum of multiple random variables is the sum over the corresponding covariance matrix. As we combine variables that follow a standard normal distribution, we can derive the individual covariances in our setup as follows: When random variables from two independent standard normal distributions are compared, (e.g. Z1 comes from the comparison C1 vs. C2 and Z2 comes from the comparison C3 vs. C4) the covariance is equal to 0. When random variables that share one sample are compared (e.g. Z1 comes from the comparison C1 vs. C2 and Z2 comes from the comparison C1 vs. C3) it can be shown that the covariance is equal to 0.5 (Ammar et al., 2019). This then allows us to determine $\sigma_{\mathcal{C}}$ and therefore Z_i^D.

Subsequently, Box1, step 3, we merged the datasets $\mathcal{D}$ that were available for each type of perturbation *P* (i.e. each of the CARLS perturbations). Depending on the perturbation, the number of available datasets varied – for example, for the C perturbation, we had three datasets ($\mathcal{D}_C = \{C_{\text{carbon sources}}, C_{\text{chemostat}}, C_{\text{titration}}\}$), while for the A perturbation, we had only one dataset ($\mathcal{D}_A = \{A_{\text{titration}}\}$). To obtain a normalized Z value for each perturbation, we used the equation

$$Z_j^P = \frac{1}{\sigma_{\mathcal{D}}} \sum_{i\in\mathcal{D}} Z_i^D \qquad \text{(eq. 3)}$$

where Z_j^P corresponds to the normalized Z-value of j-th Perturbation P. The value is normalized by the standard deviation over the datasets $\mathcal{D}$, denoted as $\sigma_{\mathcal{D}}$. The calculation is again carried out via the summation over the covariance matrix. However, because the random variables Z_i^D are independent from each other, all covariances are zero except for the covariances of the random variables with themselves (i.e. their variances). Because each Z_i^D is (0,1) normalized according to eq. 2, the resulting variance corresponds simply to the number of elements in $\mathcal{D}$ and $\sigma_{\mathcal{D}}$ is therefore

592 the square root of the number of elements n in $\mathcal{D}$. In the case that $\mathcal{D}$ contains only one element, for
593 example in the $\mathcal{D}_A$ case, $Z_j^P = Z_i^D$.
594
595 For the final calculation of the Survival score Box1, step 4, the set of perturbations $\mathcal{P}$ is
596 summarized to the Survival score Z^S via the equation:

$$Z^S = \frac{1}{\sigma_{\mathcal{P}}} \sum_{j \in \mathcal{P}} Z_j^P \qquad \text{(eq. 4)}$$

597
598 The standard deviation $\sigma_{\mathcal{P}}$ is the square root of the number of elements in $\mathcal{P}$, following the same
599 reasoning as above. The overall score is robust against missing values, as perturbations that are
600 not available (e.g. if for a certain protein X, we have only $\mathcal{P} = \{\mathrm{C}, \mathrm{R}, \mathrm{L}, \mathrm{S}\}$ available) also do not
601 contribute to $\sigma_{\mathcal{P}}$. The available Z-values then contribute more strongly to the overall score.
602
603 *Absolute quantification of proteins*
604 For absolute quantification, we used protein synthesis rates derived by (Li et al., 2014) from
605 ribosomal sequencing data of a MG1655 glucose reference condition. Synthesis rates were used
606 as proxies for copy numbers and multiplied by the respective molecular weights to obtain mass
607 estimates. Further conditions were compared relatively to the reference with MS-EmpiRe and the
608 mass estimates were scaled by the respective fold changes. To determine the mass fraction of a
609 gene set, the genes of the set were summed and divided by summed mass of all genes.
610
611 *GO enrichment analyses*
612 The Gene Ontology (GO) was downloaded from http://geneontology.org (03/2019) together with
613 the *E. coli* "ecocyc.gaf" annotation. The relations "is_a" and "part_of" were used for the
614 construction of the gene sets. Score-based analysis was carried out using the Kolmogorov-Smirnov
615 test with signed scores. Multiple testing correction was carried out via the Benjamini-Hochberg
616 procedure.
617
618 **Acknowledgements**
619 This project was supported by MIRA grant (5R35GM137895) and an HMS Junior Faculty
620 Armenise grant to MB. SJS was supported by EMBO via a Long-term fellowship (ALTF 782-

2017) and HFSP via a long-term fellowship (LT000597/2018). CA was supported by a PhD scholarship of the Deutsche Forschungsgemeinschaft (DFG, Graduate School QBM).

Author contribution

SJS, CA and MB conceived the project. SJS and CA performed experiments and proteomics analysis. YFC constructed strains. RZ supervised proteomics analysis. SJS, CA, RZ and MB wrote the paper.

Conflicts of interest

The authors declare that they have no conflict of interest.

Data availability

The uploaded Source Data contains the data underlying each figure ("Figure Data.zip"). The proteomics raw data can be found under the repositories specified in the references. Code and data for bioinformatics analyses are available on Github (https://github.com/ammarcsj/ecoli_survival_scoring).

References

Almirón, M., Link, A.J., Furlong, D., and Kolter, R. (1992). A novel DNA-binding protein with regulatory and protective roles in starved Escherichia coli. Genes Dev *6*, 2646–2654. https://doi.org/10.1101/gad.6.12b.2646.

Ammar, C., Gruber, M., Csaba, G., and Zimmer, R. (2019). MS-EmpiRe Utilizes Peptide-level Noise Distributions for Ultra-sensitive Detection of Differentially Expressed Proteins. Molecular & Cellular Proteomics *18*, 1880–1892. https://doi.org/10.1074/mcp.RA119.001509.

Baba, T., Ara, T., Hasegawa, M., Takai, Y., Okumura, Y., Baba, M., Datsenko, K.A., Tomita, M., Wanner, B.L., and Mori, H. (2006). Construction of *Escherichia coli* K-12 in-frame, single-gene knockout mutants: the Keio collection. Mol Syst Biol *2*. https://doi.org/10.1038/msb4100050.

Basan, M., Zhu, M., Dai, X., Warren, M., Sévin, D., Wang, Y.-P., and Hwa, T. (2015a). Inflating bacterial cells by increased protein synthesis. Mol Syst Biol *11*. https://doi.org/10.15252/msb.20156178.

Basan, M., Hui, S., Okano, H., Zhang, Z., Shen, Y., Williamson, J.R., and Hwa, T. (2015b). Overflow metabolism in Escherichia coli results from efficient proteome allocation. Nature *528*, 99–104. https://doi.org/10.1038/nature15765.

654 Biselli, E., Schink, S.J., and Gerland, U. (2020). Slower growth of Escherichia coli leads to longer
655 survival in carbon starvation due to a decrease in the maintenance rate. Molecular Systems
656 Biology *16*, e9478. https://doi.org/10.15252/msb.20209478.

657 Bremer, H., and Dennis, P.P. (2008). Modulation of Chemical Composition and Other
658 Parameters of the Cell at Different Exponential Growth Rates. EcoSal Plus *3*.
659 https://doi.org/10.1128/ecosal.5.2.3.

660 Bryant, J.A., Morris, F.C., Knowles, T.J., Maderbocus, R., Heinz, E., Boelter, G., Alodaini, D.,
661 Colyer, A., Wotherspoon, P.J., Staunton, K.A., et al. (2020). Structure of dual BON-domain
662 protein DolP identifies phospholipid binding as a new mechanism for protein localisation. Elife
663 *9*, e62614. https://doi.org/10.7554/eLife.62614.

664 Carpenter, A.E., Jones, T.R., Lamprecht, M.R., Clarke, C., Kang, I.H., Friman, O., Guertin, D.A.,
665 Chang, J.H., Lindquist, R.A., Moffat, J., et al. (2006). CellProfiler: image analysis software for
666 identifying and quantifying cell phenotypes. Genome Biol *7*, R100. https://doi.org/10.1186/gb-
667 2006-7-10-r100.

668 Chiang, S.M., and Schellhorn, H.E. (2012). Regulators of oxidative stress response genes in
669 Escherichia coli and their functional conservation in bacteria. Archives of Biochemistry and
670 Biophysics *525*, 161–169. https://doi.org/10.1016/j.abb.2012.02.007.

671 Cox, J., and Mann, M. (2008). MaxQuant enables high peptide identification rates,
672 individualized p.p.b.-range mass accuracies and proteome-wide protein quantification. Nat
673 Biotechnol *26*, 1367–1372. https://doi.org/10.1038/nbt.1511.

674 Csonka, L.N., Ikeda, T.P., Fletcher, S.A., and Kustu, S. (1994). The accumulation of glutamate is
675 necessary for optimal growth of Salmonella typhimurium in media of high osmolality but not
676 induction of the proU operon. Journal of Bacteriology *176*, 6324–6333.
677 https://doi.org/10.1128/jb.176.20.6324-6333.1994.

678 Dukan, S., and Nyström, T. (1999). Oxidative Stress Defense and Deterioration of Growth-
679 arrested Escherichia coli Cells. J. Biol. Chem. *274*, 26027–26032.
680 https://doi.org/10.1074/jbc.274.37.26027.

681 Farr, S.B., and Kogoma, T. (1991). Oxidative stress responses in Escherichia coli and Salmonella
682 typhimurium. Microbiological Reviews *55*, 561–585. .

683 Farr, S.B., Touati, D., and Kogoma, T. (1988). Effects of oxygen stress on membrane functions in
684 Escherichia coli: role of HPI catalase. J Bacteriol *170*, 1837–1842.
685 https://doi.org/10.1128/jb.170.4.1837-1842.1988.

686 Finkel, S.E. (2006). Long-term survival during stationary phase: evolution and the GASP
687 phenotype. Nat Rev Microbiol *4*, 113–120. https://doi.org/10.1038/nrmicro1340.

688 Fontaine, F., Stewart, E.J., Lindner, A.B., and Taddei, F. (2008). Mutations in two global
689 regulators lower individual mortality in Escherichia coli. Molecular Microbiology *67*, 2–14. .

690 Fung, T., and Kwong, N. (2013). Residual Glycogen Metabolism in Escherichia coli is Specific to
691 the Limiting Macronutrient and Varies During Stationary Phase. *17*, 5. .

692 Geiger, T., Cox, J., Ostasiewicz, P., Wisniewski, J.R., and Mann, M. (2010). Super-SILAC mix for
693 quantitative proteomics of human tumor tissue. Nat Methods *7*, 383–385.
694 https://doi.org/10.1038/nmeth.1446.

695 Hengge-Aronis, R., and Fischer, D. (1992). Identification and molecular analysis of glgS, a novel
696 growth-phase-regulated and rpoS-dependent gene involved in glycogen synthesis in Escherichia
697 coli. Molecular Microbiology *6*, 1877–1886. https://doi.org/10.1111/j.1365-
698 2958.1992.tb01360.x.

699 Houser, J.R., Barnhart, C., Boutz, D.R., Carroll, S.M., Dasgupta, A., Michener, J.K., Needham,
700 B.D., Papoulas, O., Sridhara, V., Sydykova, D.K., et al. (2015). Controlled Measurement and
701 Comparative Analysis of Cellular Components in E. coli Reveals Broad Regulatory Changes in
702 Response to Glucose Starvation. PLOS Computational Biology *11*, e1004400.
703 https://doi.org/10.1371/journal.pcbi.1004400.

704 Houser, J.R., Barnhart, C., Boutz, D.R., Carroll, S.M., Dasgupta, A., Michener, J.K., Needham,
705 B.D., Papoulas, O., Sridhara, V., Sydykova, D.K., et al. (2015). PRIDE PXD002140
706 (https://www.ebi.ac.uk/pride/ PXD002140) [DATA SET]

707 Hui, S., Silverman, J.M., Chen, S.S., Erickson, D.W., Basan, M., Wang, J., Hwa, T., and Williamson,
708 J.R. (2015). Quantitative proteomic analysis reveals a simple strategy of global resource
709 allocation in bacteria. Molecular Systems Biology *11*, 784.
710 https://doi.org/10.15252/msb.20145697.

711 Hui, S., Silverman, J.M., Chen, S.S., Erickson, D.W., Basan, M., Wang, J., Hwa, T., and Williamson,
712 J.R. (2015). PRIDE PXD001467 (https://www.ebi.ac.uk/pride/ PXD001467) [DATA SET]
713
714 Irving, S.E., Choudhury, N.R., and Corrigan, R.M. (2021). The stringent response and
715 physiological roles of (pp) pGpp in bacteria. Nature Reviews Microbiology *19*, 256–271. .

716 Li, G.-W., Burkhardt, D., Gross, C., and Weissman, J.S. (2014). Quantifying Absolute Protein
717 Synthesis Rates Reveals Principles Underlying Allocation of Cellular Resources. Cell *157*, 624–
718 635. https://doi.org/10.1016/j.cell.2014.02.033.

719 Magnusson, L.U., Nyström, T., and Farewell, A. (2003). Underproduction of ç70 Mimics a
720 Stringent Response: A PROTEOME APPROACH *. Journal of Biological Chemistry *278*, 968–973.
721 https://doi.org/10.1074/jbc.M209881200.

722 Makman, R.S., and Sutherland, E.W. (1965). Adenosine 3',5'-Phosphate in Escherichia coli. J Biol
723 Chem *240*, 1309–1314. .

724 Malinverni, J.C., and Silhavy, T.J. (2009). An ABC transport system that maintains lipid
725 asymmetry in the Gram-negative outer membrane. Proceedings of the National Academy of
726 Sciences *106*, 8009–8014. https://doi.org/10.1073/pnas.0903229106.

727 McBroom, A.J., Johnson, A.P., Vemulapalli, S., and Kuehn, M.J. (2006). Outer membrane vesicle
728 production by Escherichia coli is independent of membrane instability. J Bacteriol *188*, 5385–
729 5392. https://doi.org/10.1128/JB.00498-06.

730 McLaughlin, S. (1972). The mechanism of action of DNP on phospholipid bilayer membranes. J
731 Membr Biol *9*, 361–372. https://doi.org/10.1007/BF01868062.

732 Moore, R.A., Bates, N.C., and Hancock, R.E. (1986). Interaction of polycationic antibiotics with
733 Pseudomonas aeruginosa lipopolysaccharide and lipid A studied by using dansyl-polymyxin.
734 Antimicrob Agents Chemother *29*, 496–500. .

735 Mori, M., Zhang, Z., Banaei-Esfahani, A., Lalanne, J.-B., Okano, H., Collins, B.C., Schmidt, A.,
736 Schubert, O.T., Lee, D.-S., Li, G.-W., et al. (2021). From coarse to fine: the absolute Escherichia
737 coli proteome under diverse growth conditions. Molecular Systems Biology *17*, e9536. .

738 Muffler, A., Fischer, D., Altuvia, S., Storz, G., and Hengge-Aronis, R. (1996). The response
739 regulator RssB controls stability of the sigma(S) subunit of RNA polymerase in Escherichia coli.
740 The EMBO Journal *15*, 1333–1339. .

741 Neidhardt, F.C. (1996). Escherichia coli and Salmonella: Cellular and Molecular Biology
742 (Washington, D.C: ASM Press).

743 Nguyen, D., Joshi-Datar, A., Lepine, F., Bauerle, E., Olakanmi, O., Beer, K., McKay, G., Siehnel, R.,
744 Schafhauser, J., Wang, Y., et al. (2011). Active Starvation Responses Mediate Antibiotic
745 Tolerance in Biofilms and Nutrient-Limited Bacteria. Science *334*, 982–986.
746 https://doi.org/10.1126/science.1211037.

747 Notley-McRobb, L., Death, A., and Ferenci, T. (1997). The relationship between external glucose
748 concentration and cAMP levels inside Escherichia coli: implications for models of
749 phosphotransferase-mediated regulation of adenylate cyclase. Microbiology (Reading) *143 (Pt
750 6)*, 1909–1918. https://doi.org/10.1099/00221287-143-6-1909.

751 Phaiboun, A., Zhang, Y., Park, B., and Kim, M. (2015). Survival Kinetics of Starving Bacteria Is
752 Biphasic and Density-Dependent. PLOS Computational Biology *11*, e1004198.
753 https://doi.org/10.1371/journal.pcbi.1004198.

754 Rojas, E.R., Billings, G., Odermatt, P.D., Auer, G.K., Zhu, L., Miguel, A., Chang, F., Weibel, D.B.,
755 Theriot, J.A., and Huang, K.C. (2018). The outer membrane is an essential load-bearing element
756 in Gram-negative bacteria. Nature *559*, 617–621. https://doi.org/10.1038/s41586-018-0344-3.

757 Schaechter, M., MaalØe, O., and Kjeldgaard, N.O. (1958). Dependency on Medium and
758 Temperature of Cell Size and Chemical Composition during Balanced Growth of Salmonella
759 typhimurium. Microbiology, *19*, 592–606. https://doi.org/10.1099/00221287-19-3-592.

760 Schäfer, U., Beck, K., and Müller, M. (1999). Skp, a molecular chaperone of gram-negative
761 bacteria, is required for the formation of soluble periplasmic intermediates of outer membrane
762 proteins. J Biol Chem *274*, 24567–24574. https://doi.org/10.1074/jbc.274.35.24567.

763 Schink, S., Polk, M., Athaide, E., Mukherjee, A., Ammar, C., Liu, X., Oh, S., Chang, Y.-F., and
764 Basan, M. (2022). The energy requirements of ion homeostasis determine the lifespan of
765 starving bacteria. 2021.11.22.469587. https://doi.org/10.1101/2021.11.22.469587. [PREPRINT]

766 Schink, S.J., Biselli, E., Ammar, C., and Gerland, U. (2019). Death Rate of E. coli during Starvation
767 Is Set by Maintenance Cost and Biomass Recycling. Cell Systems *9*, 64-73.e3.
768 https://doi.org/10.1016/j.cels.2019.06.003.

769 Schmidt, A., Kochanowski, K., Vedelaar, S., Ahrné, E., Volkmer, B., Callipo, L., Knoops, K., Bauer,
770 M., Aebersold, R., and Heinemann, M. (2016). The quantitative and condition-dependent
771 Escherichia coli proteome. Nat Biotechnol *34*, 104–110. https://doi.org/10.1038/nbt.3418.

772 Schmidt, A., Kochanowski, K., Vedelaar, S., Ahrné, E., Volkmer, B., Callipo, L., Knoops, K., Bauer,
773 M., Aebersold, R., and Heinemann, M. (2016). PRIDE PXD000498 (https://www.ebi.ac.uk/pride/
774 PXD000498) [DATA SET]

775 Schneck, E., Schubert, T., Konovalov, O.V., Quinn, B.E., Gutsmann, T., Brandenburg, K., Oliveira,
776 R.G., Pink, D.A., and Tanaka, M. (2010). Quantitative determination of ion distributions in
777 bacterial lipopolysaccharide membranes by grazing-incidence X-ray fluorescence. PNAS *107*,
778 9147–9151. https://doi.org/10.1073/pnas.0913737107.

779 Shi, H., Westfall, C.S., Kao, J., Odermatt, P.D., Anderson, S.E., Cesar, S., Sievert, M., Moore, J.,
780 Gonzalez, C.G., Zhang, L., et al. (2021). Starvation induces shrinkage of the bacterial cytoplasm.
781 Proc Natl Acad Sci USA *118*, e2104686118. https://doi.org/10.1073/pnas.2104686118.

782 Soupene, E., van Heeswijk, W.C., Plumbridge, J., Stewart, V., Bertenthal, D., Lee, H., Prasad, G.,
783 Paliy, O., Charernnoppakul, P., and Kustu, S. (2003). Physiological Studies of Escherichia coli
784 Strain MG1655: Growth Defects and Apparent Cross-Regulation of Gene Expression. J Bacteriol
785 *185*, 5611–5626. https://doi.org/10.1128/JB.185.18.5611-5626.2003.

786 Steinhaus, E.A., and Birkeland, J.M. (1939). Studies on the Life and Death of Bacteria. J Bacteriol
787 *38*, 249–261. .

788 Strange, R.E. (1968). Bacterial “Glycogen” and Survival. Nature *220*, 606–607.
789 https://doi.org/10.1038/220606a0.

790 Suzuki, H., Nishimura, Y., Yasuda, S., Nishimura, A., Yamada, M., and Hirota, Y. (1978). Murein-
791 lipoprotein of Escherichia coli: a protein involved in the stabilization of bacterial cell envelope.
792 Mol Gen Genet *167*, 1–9. https://doi.org/10.1007/BF00270315.

793 Tsang, M.-J., Yakhnina, A.A., and Bernhardt, T.G. (2017). NlpD links cell wall remodeling and
794 outer membrane invagination during cytokinesis in Escherichia coli. PLoS Genet *13*, e1006888.
795 https://doi.org/10.1371/journal.pgen.1006888.

796 Yem, D.W., and Wu, H.C. (1978). Physiological characterization of an Escherichia coli mutant
797 altered in the structure of murein lipoprotein. J Bacteriol *133*, 1419–1426.
798 https://doi.org/10.1128/jb.133.3.1419-1426.1978.

799 You, C., Okano, H., Hui, S., Zhang, Z., Kim, M., Gunderson, C.W., Wang, Y.-P., Lenz, P., Yan, D.,
800 and Hwa, T. (2013). Coordination of bacterial proteome with metabolism by cAMP signalling.
801 Nature *500*, 301–306. https://doi.org/10.1038/nature12446.

802 Zambrano, M.M., and Kolter, R. (1996). GASPing for Life in Stationary Phase. Cell *86*, 181–184.
803 https://doi.org/10.1016/S0092-8674(00)80089-6.

804
805

Expanded View Figures Legends

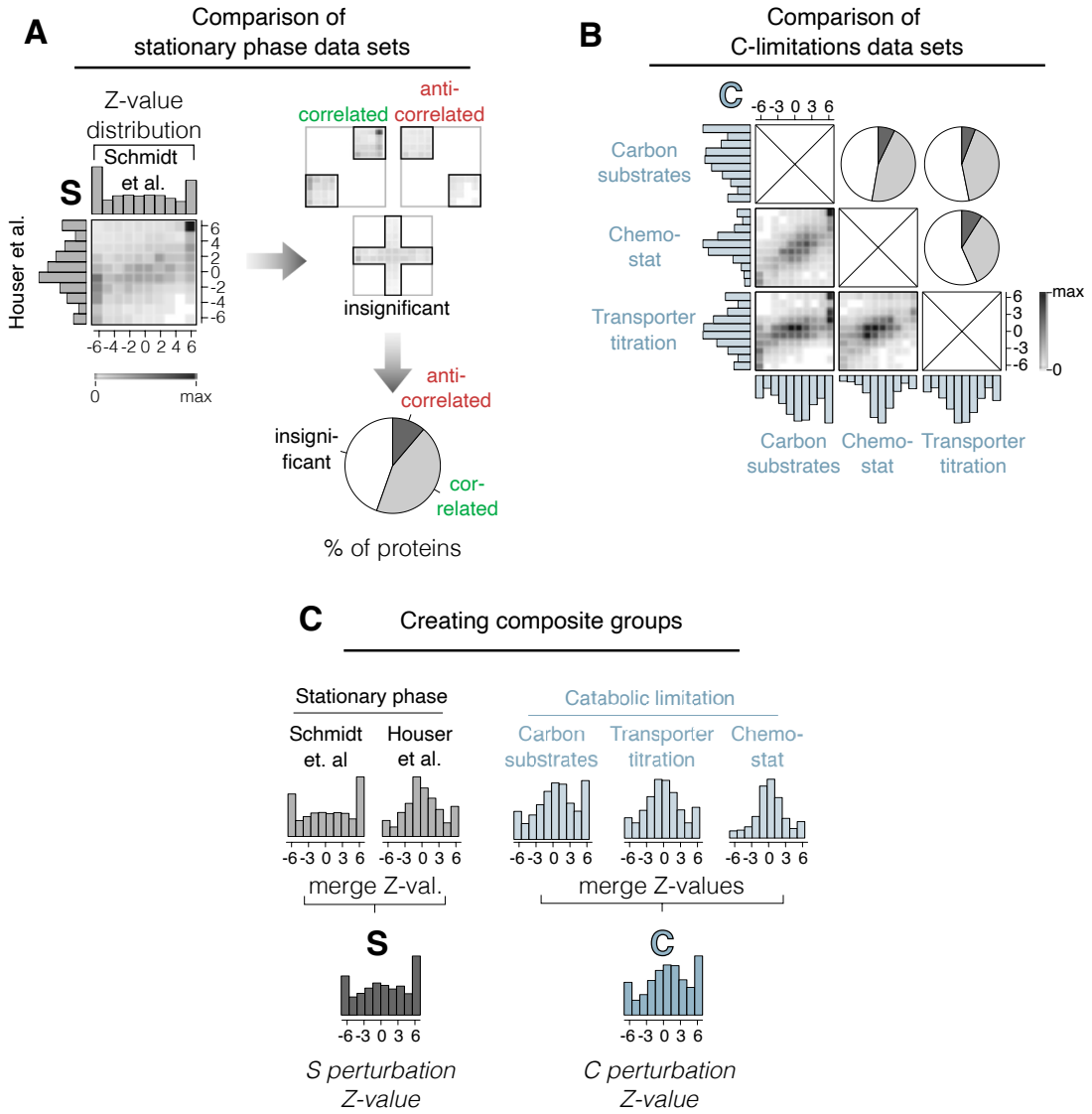

Figure EV1 Comparison and merging of MS proteomics data from different sources. (**A**) Comparison of Z-value distributions from two different data sets, by Houser et al. (Data ref: Houser et al., 2015) and Schmidt et al. (Data ref: Schmidt et al., 2016), both measured in stationary phase after growth on glucose. On left: Z-value distributions of individual experiments are shown on left and top of correlogram. Shaded area inside the correlogram depicts frequency distribution of individual proteins that are measured in both data sets. On right: Proteins scored in top right and bottom left corner are counted 'correlated', proteins in the top left and bottom right are counted as 'uncorrelated'. Cut-off for significance is chosen at Z = 1.28, corresponding to a p-value of 0.1. Proteins with at least one Z-value less than 1.28 are counted as uncorrelated. On bottom: Quantitative analysis of correlation. Only a minority of proteins are observed to anti-correlate between data sets, with the majority either correlating or being statistically insignificant. (**B**) Analysis of correlograms and quantification in pie charts of three data sets of different catabolic limitation analog to panel A. 'Carbon substrates' and 'chemostat' taken from Schmidt et al (Data ref: Schmidt et al., 2016), 'Transporter titration' taken from Hui et al (Data ref: Hui et al., 2015). Different types of catabolic limitation show high correlation between data sets. (**C**) Data sets from panel A and B, respectively, are merged to form a single Z-value distribution for each growth perturbation.

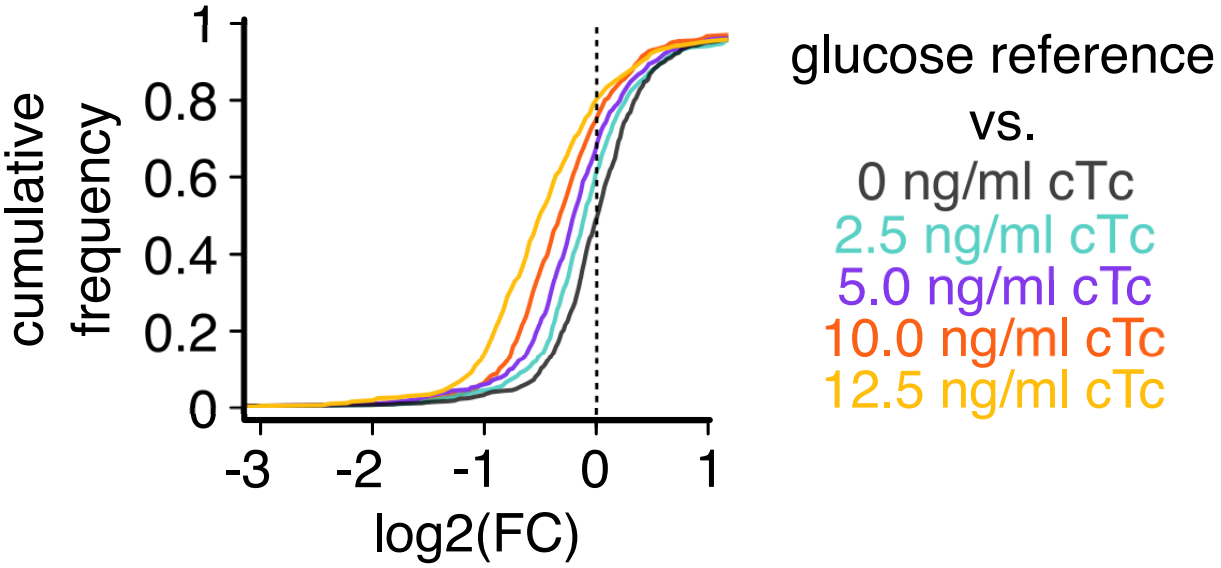

Figure EV2 Cumulative distribution of fold-changes under expression of a useless protein (O condition). Fold-change of protein abundances (FC) in LacZ overexpression using strain NQ1389 compared to the reference condition of wild-type *E. coli* grown on glucose. The abundance of vast majority of proteins decreases with induction of LacZ (inducer: chlortetracycline, cTc).

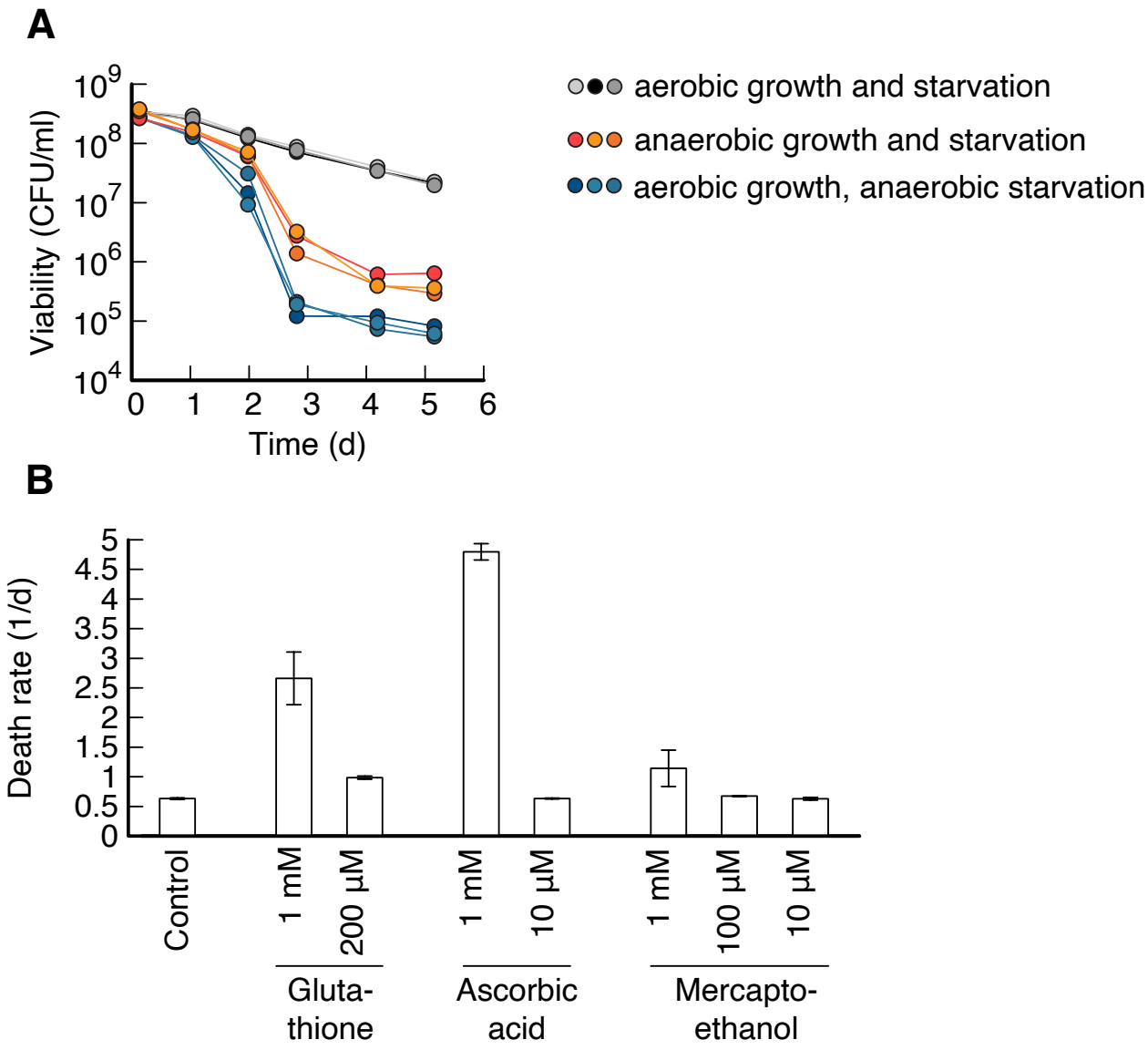

***Figure* EV*3* Starvation in the absence of oxidative damage.** (**A**) Viability over time in E. coli cultures starved in either anaerobic or aerobic conditions. Cultures previously grown on glucose minimal medium. Neither performing both starvation and growth (orange), nor only starvation in anaerobic conditions (blue) decreased death rate. Instead in both cases, viability decreased several orders of magnitude more compared to aerobic conditions. This finding is in disagreement with previous claims that anaerobic starvation prevents loss of viability (Dukan and Nyström, 1999), but matches the observation that bacteria actively recycle nutrients from dead cells (Schink et al., 2019), which is more efficient if bacteria can use respiration. (**B**) Starvation in the presence of antioxidants glutathione, ascorbic acid (Vitamin C) and beta-mercaptothanol. High concentrations of antioxidants increase death rate, while low concentrations show no significant effect over control. No antioxidant condition significantly decreased death rate.

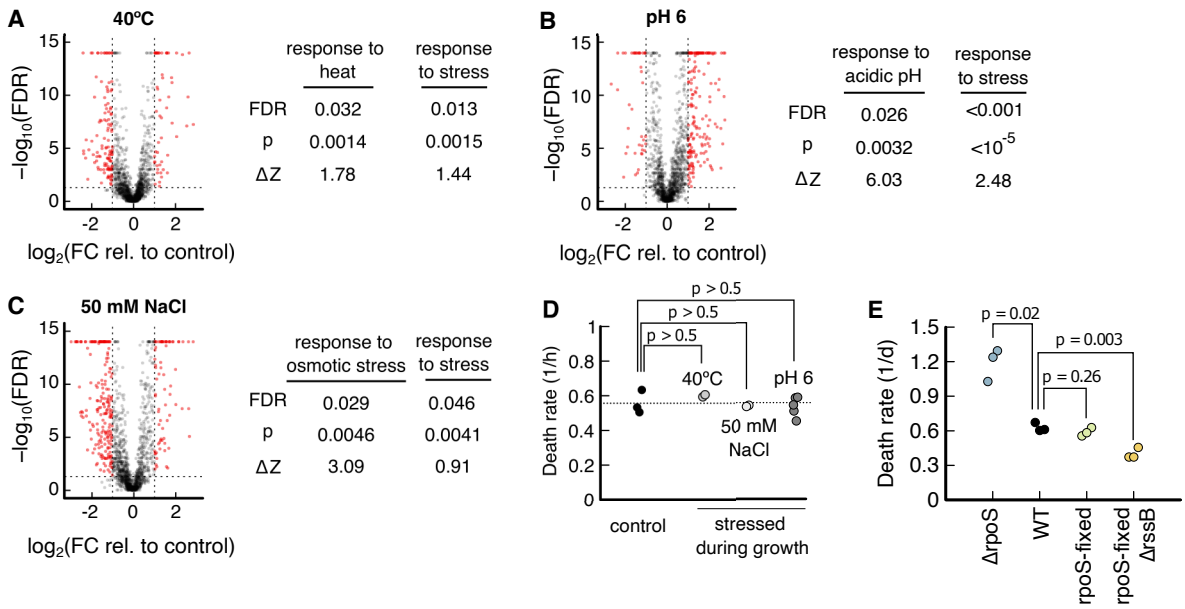

Figure EV4 Effect of pre-stressing on proteome and survival kinetics. (**A-C**) Comparison of stress conditions to a glucose reference. On left side of each panel, volcano plots of individual proteins, showing the probability of being a response versus the logarithm of the fold change. Proteins with fold change higher than 2, i.e., $log_2(2) = 1$, and false discovery rate smaller than 0.05, i.e. $log_{10}(0.05) = -1.3$, are colored in red. On the right side of the panel, for each pre-stress (40ºC, pH 6 and 50 mM NaCl), the corresponding stress response and the general 'response to stress' are tested for significant upregulation using Kolmogorov-Smirnov tests. In each pre-stress, both the specific and the general stress response are significantly upregulated, FDR < 0.05. Data source: (Data ref: Schmidt et al., 2016). (**D**) After stressing during growth, bacteria are transferred to pre-warmed, carbon-free minimal medium without stress. Death rates of neither pre-stressing condition led to a significant change in death rate, p> 0.5. (**E**) Death rate of wild-type NCM3722 compared to ΔrpoS, a 'rpoS-fixed' strain where an amber stop codon in *rpoS* is restored (Mori et al., 2021) and a strain with 'rpoS-fixed' and ΔrssB. All mutants have NCM3722 as background. p-values in panels D and E are calculated using a two-tailed t-test.

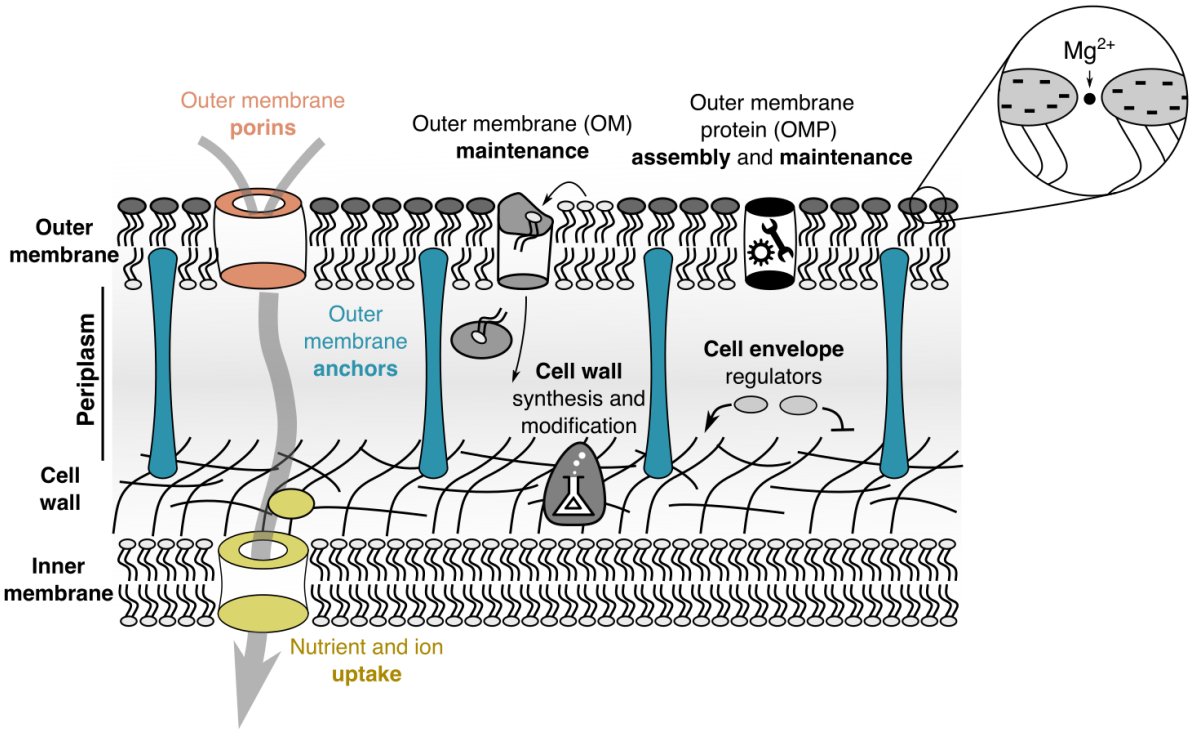

858

859 **Figure EV5 The cell envelope of *E. coli*.** For gram-negative bacteria, the cell envelope consists of the
860 outer membrane, the cell wall, and space between inner and outer membrane called periplasm. Proteins in
861 the cell envelope have diverse functions. Outer membrane anchors (blue), specifically Lpp and OmpA,
862 connect the outer membrane to the cell wall. Outer membrane porins (red) are large tunnel-shaped proteins
863 that facilitate diffusion of biomolecules and ions across the outer membrane. Nutrient uptake systems
864 (yellow) import biomolecules and ions across the inner membrane. While most of the nutrient uptake
865 system is in the inner membrane, thus not considered as part of the envelope, binding proteins (yellow circle
866 in periplasm) are. There are over 100 different kinds of binding proteins in *E. coli*, which make up a
867 significant fraction of the proteome of the cell envelope. Other proteins include proteins involved in
868 maintenance of the outer membrane, e.g. the Mla system which shuffles phospholipids from the outer leaflet
869 of the outer membrane to the inner membrane. Outer membrane protein (OMP) assembly and maintenance
870 are proteins that fold outer membrane proteins, e.g. Bam complex, proteases which degrade misfolded
871 proteins, e.g. DegP, and chaperones that prevent folding of outer membrane proteins in solution, e.g. Skp.
872 Cell envelope regulators include the CpxAR signal transduction system and regulation of RpoE via anti-
873 sigma factor RseA. Cell wall synthesis and modification includes cell wall hydrolases and regulators of cell
874 wall synthesis. Lipid A, the lipid on the outer leaflet of the outer membrane is highly charged and requires
875 Mg2+ ions for shielding (Schneck et al., 2010).

876

877 **Supporting Information Tables**

878

879 All Supporting Information Tables are provided in the single excel file
880 "SupportingInformationTables.xlsx" with individual sheets for Tables S1 to S5.

881

882 **Table S1**. Growth and death rates in different growth perturbations. Coloring corresponds to Fig.
883 1. For all conditions listed here, cultures were washed and resuspended in carbon-free medium.
884 All strains are derived from wild-type *E. coli* K-12 NCM3722. The titratable glutamate synthesis
885 strain NQ393 contains a deletion of gdhA and the promotor of gltBD is replaced by P_{lac}, which is
886 induced with Isopropyl β-D-1-thiogalactopyranoside (IPTG) (Hui et al., 2015). Strain NQ1389
887 contains two plasmids, P_{tet}-tetR on pZA31 and $P_{tetstab}$-lacZ on pZE1, induced by
888 Chlortetracycline (cTc), allowing high levels of superfluous LacZ expression (Basan et al.,
889 2015a). In addition to Fig. 1A, the table also includes data from a titratable lactose uptake strain
890 NQ381 has the P_{lac} replaced by Pu, which is induced with 3-methylbenzyl alcohol (3MBA) (You
891 et al., 2013). This data follows the same trend as other carbon limitations but is not shown in Fig.
892 1A.

893

894 **Table S2**. List of Z values, Survival scores and fold-changes of abundance in pre-stress
895 conditions. A total of 2039 proteins were scored. Values indicated with NA are not available. See
896 Methods for details on the calculation of Z values and Survival scores. The CARLS columns
897 show the Z values derived as described in the methods. For the C and the S conditions, several
898 data sets were available, which were merged as visualized in Figure S2. The Z values for the
899 individual data sets are also listed as follows: C_chemostat is the chemostat conditions of (Data
900 ref. Schmidt et al., 2016), C_carbon_sources is the different carbon growth conditions of (Data
901 ref: Schmidt et al., 2016), C_glucose_uptake_titration is the glucose transporter titration set
902 from (Data ref: Hui et al., 2015) 'S_houser' is the Z values after 48 h of stationary phase
903 respectively in the study of (Data ref: Houser et al., 2015) 'S_schmidt' is the Z values of the
904 stationary phase condition of. (Data ref: Schmidt et al., 2016). 'HEAT', 'OSM' and 'pH' are Z
905 values of pre-stress conditions with 42ºC, 50mM NaCl and pH 6, respectively, of (Data ref:
906 Schmidt et al., 2016). 'FC CHvsOSM', 'FC CHvsHEAT' and 'FC CHvsPH' are the fold-

907 changes of protein abundances in pre-stress conditions compared to reference glucose conditions,
908 which are used in Fig. EV4.
909
910 **Table S3**. Full list of GO processes and GO compartments and their False discovery rates (FDR)
911 and median Survival scores.

912 **Table S4**. Absolute abundances of cell envelope proteins, and protein groups in stationary phase,
913 glucose reference condition and LB. See Methods for details on the quantification.

914 **Table S5**. Results from a knock-out screen. Genes were chosen to have high Survival scores and
915 to be non-essential. Note that these genes were selected based on a preliminary version of the
916 proteomics analysis, meaning that they do not 100% overlap with the highest scoring set of genes
917 of Table S2. Survival scores of the final analysis are given in column D. Cultures were grown in
918 N-C- supplemented with NH_4Cl and 20mM glycerol in 96 well plates and starved by letting
919 glycerol deplete. Death rate is estimated from a measurement of viability after glycerol ran out
920 and a measurement after five days of starvation. Each data point is from a single experiment, and
921 the hits were independently verified (Fig. 2). Out of the top five genes, three (*lpp*, *bamE* and
922 *mlaC*) are essential for the cell envelope integrity.